Volume 3
Number 5
May 2024
Pages 711–884

Sensors & Diagnostics

rsc.li/sensors

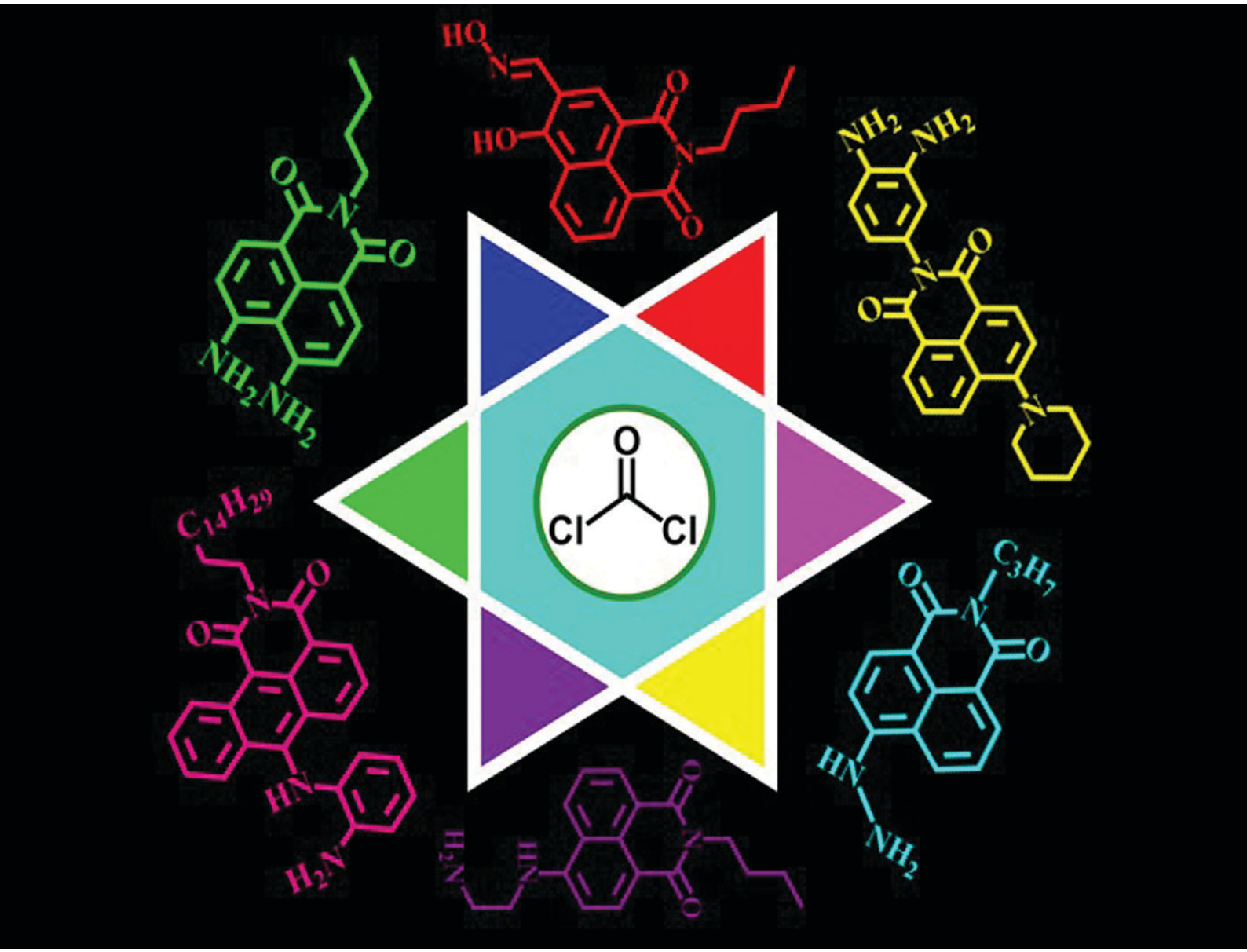

ISSN 2635-0998

ROYAL SOCIETY OF CHEMISTRY

TUTORIAL REVIEW

Thorfinnur Gunnlaugsson, Sankarasekaran Shanmugaraju *et al.*
Reactivity-based amino-1,8-naphthalimide fluorescent chemosensors for the detection and monitoring of phosgene

Sensors & Diagnostics

TUTORIAL REVIEW

View Article Online
View Journal | View Issue

Cite this: *Sens. Diagn.*, 2024, **3**, 783

Reactivity-based amino-1,8-naphthalimide fluorescent chemosensors for the detection and monitoring of phosgene

Mannanthara Kunhumon Noushija,[a] Alenthwar Vamshi Krishna,[a] Thorfinnur Gunnlaugsson *[bc] and Sankarasekaran Shanmugaraju *[a]

Phosgene (carbonyl dichloride, $COCl_2$) is an extremely toxic and hazardous chemical warfare agent (CWA; schedule 3 substance) that poses significant threats to public safety and human well-being. Simultaneously, it is a commonly employed reagent in chemical synthesis in laboratories and industrial settings. Therefore, monitoring phosgene concentration levels is essential for handling them within the workplace and for safeguarding public security. Activity-based fluorescent probes are the most effective real-time detection methods currently used for the detection of CWAs. Reaction-based sensing offers excellent temporal and spatial resolution, minimal side effects, and quick response times. Recently, a plethora of reaction-based fluorescent probes have been designed for the detection of phosgene. This review provides an overview of the latest developments using amino-1,8-naphthalimide-based small-molecule fluorescent probes designed for phosgene detection/sensing. Additionally, we investigate the existing challenges and prospects in the field of reaction-based fluorescent probes for phosgene detection. Herein, various fluorescence sensors are categorized based on their reactions with phosgene, and each section highlights the reaction sites, sensing mechanisms, structure–function relationships, photophysical performances, and practical applications of these sensors. It is our aspiration that this review will provide valuable insights into the advancement of cutting-edge fluorescent probes tailored for phosgene detection and sensing.

Received 10th February 2024,
Accepted 25th March 2024

DOI: 10.1039/d4sd00048j

rsc.li/sensors

[a] *Department of Chemistry, Indian Institute of Technology Palakkad, Palakkad-678557, Kerala, India. E-mail: shanmugam@iitpkd.ac.in*
[b] *School of Chemistry and Trinity Biomedical Sciences Institute (TBSI), Trinity College Dublin, The University of Dublin, Dublin 2, Ireland. E-mail: gunnlaut@tcd.ie*
[c] *Advanced Materials and BioEngineering Research (AMBER) Centre, Trinity College Dublin, The University of Dublin, Dublin 2, Ireland*

1. Introduction

Chemical warfare agents (CWAs) have earned a notorious reputation on the battlefield owing to their use as highly destructive weapons in significant conflicts, such as World War I and II, as well as in more recent conflicts.[1] Among the

Mannanthara Kunhumon Noushija

Ms. Mannanthara Kunhumon Noushija obtained her B.Sc. degree in Chemistry from Government Victoria College Palakkad in 2018 and her M.Sc. in Chemistry from Calicut University, Thenhippalam, Kerala, in 2020. She is currently pursuing her Ph.D. in the Department of Chemistry at the Indian Institute of Technology, Palakkad. Her research interests focus on the design and development of small-molecule fluorescent chemosensors for biologically relevant analytes.

Alenthwar Vamshi Krishna

Mr. Alenthwar Vamshi Krishna earned his BS-MS dual degree in Chemistry from the Indian Institute of Science Education and Research (IISER), Pune, in 2019. Currently, he is a Ph.D. student in the Department of Chemistry at the Indian Institute of Technology, Palakkad. His research interest focuses on polyimide-based cathode materials for battery applications.

various categories of CWAs, including pulmonary agents, blister agents, mustard agents, and nerve agents, phosgene stands out for its devastating effectiveness, which is responsible for causing up to 80% mortality during World War I.[2,3] Phosgene ($COCl_2$) is a deadly colorless gas, characterized by its violent suffocating properties, high toxicity, and mild odor.[4,5] It inflicts severe pulmonary complications, such as noncardiogenic pulmonary edema, pulmonary emphysema, and respiratory tract and lung organ damage, and can lead to fatality at elevated concentrations.[6,7] However, this chemical is also commonly employed within both chemical laboratories (at low concentrations) and industrial settings (at high concentrations) as an important reagent for use in chemical synthesis and manufacturing. Hence, there exists a good reason to generate sensors or probes that can detect and monitor this chemical in these settings.

Phosgene and its substitutes, diphosgene and triphosgene, differ significantly from other CWAs, such as nerve agents, which are subject to strict prohibition and control under relevant laws.[8] The notable distinction lies in their widespread availability within the chemical industry. These compounds are readily accessible considering their extensive utilization in various industrial applications, encompassing the production of engineering plastics, polyurethane materials, pesticides, pharmaceuticals, and other materials.[9,10] Consequently, the combination of its lethal nature and extensive industrial usage makes phosgene susceptible to accidental releases during industrial incidents or, in a worst-case scenario, its deliberate utilization for illegal activities.[11] Due to its extreme toxicity, phosgene represents substantial dangers to both global security and public health.[12] Consequently, extensive endeavors have been undertaken to develop selective and sensitive techniques for the detection of this hazardous substance.

High-performance liquid chromatography (HPLC),[13] gas chromatography (GC),[14] and gas chromatography-mass spectrometry (GC-MS)[15–17] are some of the commonly used instruments in conventional procedures for phosgene detection. Among them, the ability of GC-MS to effectively separate, identify, and quantify analytes makes it a valuable tool for the detection of CWAs, including phosgene. However, its stationary nature, cost, and the need for complex sample pre-treatment before sample analysis limits its on-site detection capabilities, while electrochemical methods have also been utilized for the determination of CWAs, and their unsatisfactory selectivity impedes practical applications.[18] Other techniques, such as infrared (IR) and Raman spectroscopies, are valuable for CWA identification, but their applications encounter challenges in detecting mixtures, particularly at low concentrations.[19–21] Each of these methods has other limitations, such as lack of portability, intricate operation, low sensitivity, or selectivity.

In contrast, fluorescent-based sensing demonstrates superior sensitivity, high selectivity, portability, and efficiency in sensing analytes, rendering them highly advantageous for the real-time detection of phosgene.[22,23] Over the past few years, researchers have made tremendous progress in the development of fluorescent chemosensors for detecting phosgene.[1,2] Until recently, several chemosensors based on classic fluorophores, such as like coumarins,[24] BODIPY,[25–28] naphthalimides,[29–32] and rhodamines,[33,34] were reported. These fluorescence probes were normally functionalized with various nucleophilic functional groups, such as amino,

Thorfinnur Gunnlaugsson

Prof. Thorfinnur (Thorri) Gunnlaugsson MRIA holds a Personal Chair as a Professor of Chemistry in the School of Chemistry, Trinity College Dublin (TCD). His research interests lie broadly within the areas of medicinal, organic and inorganic supramolecular, and materials chemistries. He is a Fellow of Trinity College Dublin and the Institute of Chemistry of Ireland and a Member of The Royal Irish Academy. In 2014, he was awarded the Institute of Chemistry of Ireland Annual Award for Chemistry and the Institute of Chemistry of Ireland (ICI) David Brown Award in 2023. He was the recipient of the Molecular Sensors and Molecular Logic Gates (MSMLG) Czarnik Award in 2021. He is the author of almost 300 papers and has an h-index of 84.

Sankarasekaran Shanmugaraju

Dr. Sankarasekaran Shanmugaraju received his B.Sc. and M.Sc. degrees in Chemistry from The American College, Madurai, and his Ph.D. degree with a gold medal for the best Ph.D. thesis from the Indian Institute of Science (IISc), Bengaluru. In 2014, he moved to Trinity College Dublin, Ireland, as an Irish Research Council (IRC) postdoctoral fellow. In 2018, he joined the Department of Chemistry at the Indian Institute of Technology Palakkad as an assistant professor. Since 2023, he has been working as an associate professor at the same institution. His group's current research activities are in the area of supramolecular structures, materials, and sensor chemistry. He is the author of almost 57 journal articles, 7 book chapters, and a book and has an h-index of 25.

hydroxyl, and sulfhydryl, that act as recognition, or reaction sites, for phosgene detection. In the phosgene, the carbonyl carbon (C═O) is extremely electrophilic and can undergo facile nucleophilic substitution reactions with various amino and hydroxyl functionalities to produce amide and ester groups, respectively.[35] Additionally, a dehydration reaction between oxime or primary amide with phosgene can result in the formation of a cyano group.[36] Simultaneously, the diamine moiety can undergo acetylation, followed by intramolecular cyclization, which can result in discernible changes in the photophysical properties of the sensor.[37]

The changes in fluorescence signal intensity are attributed to different sensing mechanisms, such as photo-induced electron transfer (PET),[38] intramolecular charge transfer (ICT),[39] excited-state intramolecular proton transfer (ESIPT),[40] and fluorescence resonance energy transfer (FRET).[41] Even though the appropriate recognition groups containing the amino (imine) or hydroxyl, *o*-phenylenediamine, catechol, 2-aminobenzylamine, ethylenediamine, oxime, acid amide, and other unexploited recognition moieties were flexibly used as recognition site in the structural design of such chemosensors and activity-based probes/sensors, the fluorophore moiety within these systems mainly plays a significant role in fluorescence-based sensing.[42,43] The judicious selection of a fluorophore decides the characteristic properties of the sensor molecules, such as its selectivity, sensitivity, photostability, quantum yields, and lifetime.[44,45]

Among the various fluorophores reported to date, the 3- or 4-amino-1,8-naphthalimides (Naps) stand out because of their special characteristics, such as straightforward synthesis, remarkable selectivity, substantial Stokes shifts, relatively high quantum yield, solvent-dependent emission characteristics, outstanding photo-stability, exceptional sensitivity, and significant interaction with analytes.[46–50] Significant advancements have been made in recent years in the development of fluorescent probes and sensors for CWAs.[1,2,51] These progressions include innovative design strategies, novel recognition elements, diverse chemical structures, as well as the creation of portable and digital sensing devices and platforms. Although a significant number of amino-1,8-naphthalimide-based fluorescence probes have been developed, no review articles have been reported to date exclusively highlighting the use of small molecule-based fluorescent chemosensors for phosgene detection based on the amino-1,8-naphthalimide structure.

This review article addresses this deficit by offering an in-depth account of the recent advances in utilizing Nap-based small-molecule chemosensors for the fluorescence detection of the phosgene. Our main focus is on the basic characteristics of such sensors and probes along with their detection, sensing methods, response capabilities, and practical applications. We aimed to provide researchers working in this exciting research field with an understanding of such sensing and an overview of the current state of the art, with the hope that they can develop new and alternative types of fluorescence-based sensing methods for detecting a range of volatile health hazards.

2. Amino-1,8-naphthalimide-based fluorescence sensors for phosgene detection

In this section, we systematically highlighted reactivity-based 3 and 4-amino-1,8-naphthalimide-based fluorescence chemosensors reported for the selective detection of phosgene, where the sensors are grouped according to their reacting functional groups.

2.1 Fluorescence sensors based on aromatic amines as recognition units

In 2016, Yoon's group synthesized the first amino-1,8-naphthalimide-based fluorescence sensor (Nap-1) for phosgene sensing based on a selective reaction of the *o*-phenylenediamine (OPD) group with the phosgene (Fig. 1).[11] The reaction of Nap-1 with the phosgene led to the formation of a corresponding electron-deficient benzimidazole derivative (Fig. 1A). This was evident from the changes in the absorption spectra and the fluorescence emission; the reaction prevented the PET process that was operational from the electron-rich OPD group to the excited state of the Nap-fluorophore before the reaction, with distinct fluorescence spectral changes where the emission was 'switched on' with a large enhancement factor. Here, a decrease in the absorption spectra centered at λ = 420 nm and a simultaneous increase in the intensity of the peak at λ = 480 nm occur upon the addition of various amounts of triphosgene (a non-volatile precursor of phosgene) to the chloroform-*p*-xylene solution of Nap-1 (Fig. 1B). From the changes in the fluorescence emission enhancement at λ = 480 nm (Fig. 1C), it was determined that the reaction was completed within 3 minutes, and the corresponding fluorescence signal ('turn-on') was detected within 30 s. Notably, sensor Nap-1 could detect phosgene concentrations as low as 2.8 ppb.

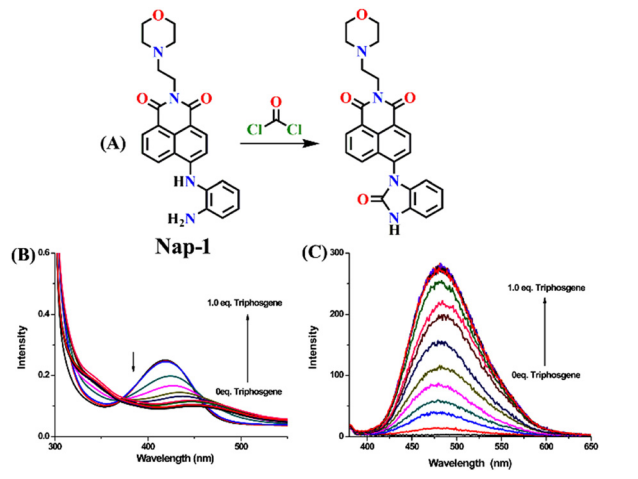

Fig. 1 (A) Structure of Nap-1 and its benzimidazole product formed after reaction with phosgene. The observed changes in (B) absorption and (C) fluorescence emission spectra of Nap-1 upon the gradual addition of the triphosgene solution. Reproduced with permission from ref. 11. Copyright 2016, American Chemical Society.

In 2017, Song and co-workers developed the first ratiometric fluorescence sensor (Nap-2) based on 4,5-diaminonaphthalimide for the visual detection of phosgene.[31] In contrast to the single-mode fluorescent sensors that either show 'turn-on' or 'turn-off', the ratiometric fluorescence sensors offer a superior and more precise solution for real-world applications. Because ratiometric sensors use two separate fluorescence signals, they can be self-calibrated by taking advantage of the two independent emission bands. This capacity makes removing outside interferences easier, significantly improving analytical data's accuracy and reliability.[52] The sensor Nap-2 underwent acylating reactions with phosgene, yielding a product with an altered ICT characteristic compared to the initial 'free' sensor (Fig. 2A). This transformation led to a notable shift in the fluorescence emission and concomitantly in color from green to blue and, hence, a ratiometric fluorescence response (Fig. 2B and C). Here, the addition of triphosgene (0 → 25 mM) (in the presence of triethylamine) caused significant changes in the fluorescence emission spectra of Nap-2, resulting in a decrease in the emission intensity at λ = 511 nm with the parallel generation of new bands at λ = 442 and 467 nm (and with a clear isoemissive point), indicating the formation of a product with weak ICT (Fig. 2B). The altered ICT transition was also reflected by the difference in the fluorescence quantum yields for Nap-2, which was determined as 0.37, and for the product, which was determined as 0.87. Nap-2 demonstrated exceptional activity-based sensing capabilities, including high sensitivity (with a limit of detection of 1.3 nM) and remarkable specificity towards phosgene in comparison to triphosgene, acyl chlorides, and nerve agent mimics. Furthermore, Nap-2 infused within a test paper was used for the gaseous phosgene sensing at a range of concentrations (0–4.0 mg L^{-1}) and the change in fluorescence color, from green to blue, was visible to the naked eye in both solution and within the test paper (Fig. 2C).

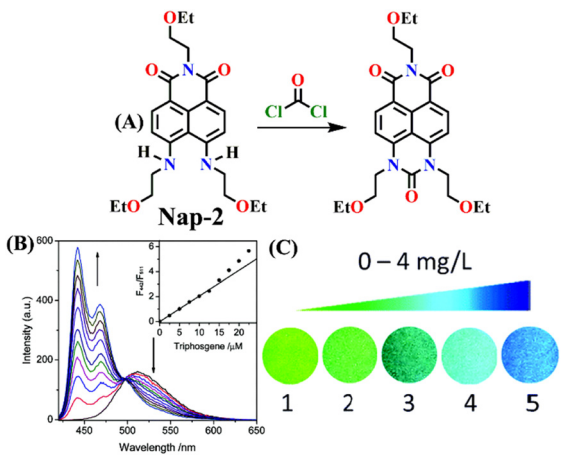

Fig. 2 (A) Structure of Nap-2 and its product upon reaction with phosgene. (B) Ratiometric fluorescence responses were observed for Nap-2 upon the gradual increase in triphosgene solution (inset: a plot of the fluorescence intensity ratio and the concentration of triphosgene). (C) Photographs of Nap-2 coated test papers after exposure to triphosgene at different concentrations. Reproduced with permission from ref. 31. Copyright 2017, the Royal Society of Chemistry.

The same group also developed sensor Nap-3 for the detection of phosgene and its analogues (diphosgene and triphosgene) in both solution and the gas phase.[30] The non-fluorescent Nap-3 effectively underwent an acylating reaction with the phosgene, resulting in the formation of a highly fluorescent product (Fig. 3A). This sensing response demonstrated a great selectivity towards the phosgene and its analogues over other analytes, such as NO, acyl chlorides, and nerve agent mimics, with the nanomolar level of sensitivity (0.2 nM for triphosgene and 0.7 nM for diphosgene). Upon the addition of varying amounts of diphosgene, the absorption band centered at λ = 436 nm decreased in absorbance, while a new blue-shifted band at λ = 411 nm emerged with a clear isosbestic point at λ = 427 nm. Nap-3 displayed a fluorescence 'turn-on' sensing response with a fluorescence emerging, enhancing at λ = 468 nm. Kinetic analysis reveals that the initial acylation of primary amines is the rate-determining step, followed by a fast-intramolecular acylation reaction. Moreover, using Nap-3, the author showed that a portable test paper could be fabricated by the authors for the sensitive detection of phosgene and its analogues, thereby achieving the detection thresholds of approximately 5 ppm through visual observation and 0.1 ppm *via* fluorescence measurements. Moreover, when Nap-3-coated test paper was exposed to various concentrations of diphosgene, the fluorescence color that changed from a faint magenta to a strong cyan was visible (Fig. 3B). These findings underscore the potential of Nap-3 as a viable fluorescence and colorimetric probe for the detection of the phosgene and its analogues, which are inexpensive for practical applications.

Subsequently, Song *et al.* reported novel fluorescent chemosensor Nap-4 for dual-mode discriminative sensing of phosgene and triphosgene.[53] Nap-4 was functionalized with a (2-(2-aminophenyl)imidazole) recognition site that could undergo two acylation reactions with the phosgene to form a green fluorescence cyclic product (Fig. 3C). In contrast, Nap-4 reacts with the triphosgene through a single acylation reaction to form a product with blue fluorescence emission (Fig. 3C); hence, these

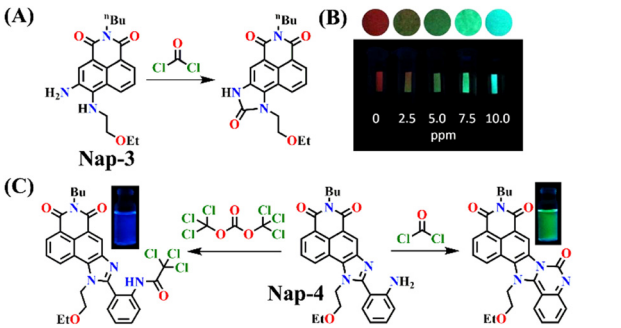

Fig. 3 (A) Structure of Nap-3 and its product upon reaction with phosgene. (B) Fluorescence images of Nap-3-coated test paper after exposure to diphosgene vapors at different concentrations. (C) The distinct reaction of Nap-4 with phosgene and triphosgene yielded green and blue-emitting products, respectively (inset: colorimetric photo). Reproduced with permission from ref. 30 and 53. Copyright 2018, Willey; 2019, American Chemical Society.

two distinct product formations were attributed to the difference in the electrophilicity between trichloromethoxycarbonyl and chlorocarbonyl. Nap-4 exhibited exceptional sensitivity, with a limit of detection (LoD) of 3.2 nM for the phosgene and 1.9 nM for the triphosgene. Additionally, it showed excellent selectivity over pertinent analytes in the solutions. Upon the addition of the triphosgene, the time-dependent UV-vis absorption and the fluorescence spectra of Nap-4 displayed a swift change in the absorption with a clear isosbestic point at λ = 285 nm and a notable enhancement in the fluorescence emission intensity centered at λ = 422 nm. Similar changes in the absorption spectra were also observed when the phosgene concentrations were increased, with a significant decrease in the absorption of the high-energy band at λ = 300–390 nm with a concomitant increase in the band at the low-energy band at λ = 390–480 nm; these changes were accommodated with an isosbestic point at λ = 390 nm. This observation demonstrates that Nap-4 has a single, efficient sensing response to the phosgene. Furthermore, the fluorescence emission spectra of Nap-4 showed a 420-fold fluorescence enhancement at λ = 526 nm. Additionally, an easy-to-use Nap-4 coated test paper, prepared by applying the electrospinning method, exhibited fast gas-phase sensing responses with an excellent sensitivity of 42 ppb towards phosgene. These studies demonstrate that Nap-4 can be a potential sensor for the ultra-trace sensing of the phosgene in both the solution and the gas phase.

In 2019, Hou and Yoon developed the fluorescent sensor Nap-5, adorned with an *o*-phenylenediamine (OPD) reactive site, for the discriminative sensing of the phosgene and the nerve agent diethyl chlorophosphite (DCP) (Fig. 4A).[8] The authors showed that when the phosgene interacts with OPD, it leads to the formation of a five-membered benzimidazolone ring. This chemical reaction effectively suppresses the ICT process by engaging the two amines in positions 4 and 5 of the Nap ring in the formation of this new heterocycle. Consequently, probe Nap-5 displayed both colorimetric and fluorescence sensing responses towards the phosgene. Upon the addition of the phosgene, the intensity of the ICT-based absorption band at λ = 520 nm decreased, which was accompanied by the appearance of two new absorption bands at λ = 462 and 438 nm, respectively (Fig. 4B). This resulted in noticeable color changes from red-brown to yellow, providing a visual means of detecting the phosgene. In the emission spectra of Nap-5, a significant enhancement in intensity at λ = 500 nm was also observed in response to the phosgene, from which a low detection limit of 72 nM was determined (Fig. 4C). Moreover, a polymeric film loaded with Nap-5 exhibited distinct optical responses for phosgene and DCP. These studies not only established a straightforward approach for the rapid and sensitive detection of CWAs but also emphasized a new strategy for developing a single fluorescent chemosensor for the simultaneous detection of two distinct analytes.

Yu and coworkers recently developed a ratiometric fluorescent sensor Nap-6 for the detection of phosgene with decent selectivity and good sensitivity (LoD = 2.25 μM).[54] Nap-6 was successfully synthesized using an active diamine as the reactive recognition site. Unlike previously reported sensors that rely on the use of *o*-phenylenediamine or diamine, both amino groups remain unaltered in Nap-6, ensuring their rapid and efficient acylation by the phosgene to form a tetrahydropyrimidin-2(1*H*)-one ring (Fig. 5A). The acylation reaction on Nap-6 effectively reduces or, to a greater extent, inhibits the Nap ICT (or the 'push-pull' effect), leading to remarkable ratiometric fluorescence responses. In the absorption spectra, a noticeable reduction in the intensity of the absorption at λ = 225 nm with a minor enhancement at the

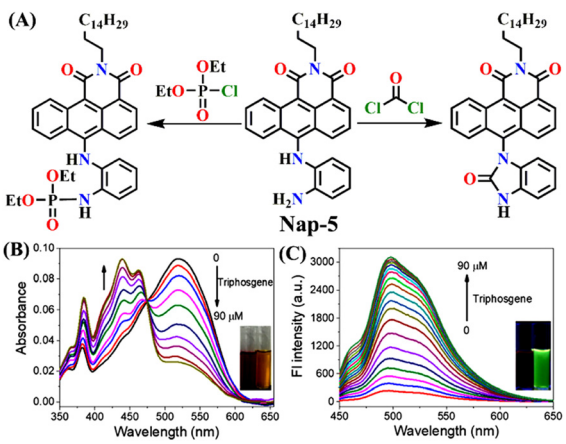

Fig. 4 (A) Structure of sensor Nap-5 and its products upon reaction with phosgene and chlorophosphite. (B) Changes in UV-visible absorption and (C) fluorescence emission spectra of Nap-5 upon the gradual addition of triphosgene in $CHCl_3$ solution (inset: visual color changes before and after the addition of triphosgene seen under UV light). Reproduced with permission from ref. 8. Copyright 2019, American Chemical Society.

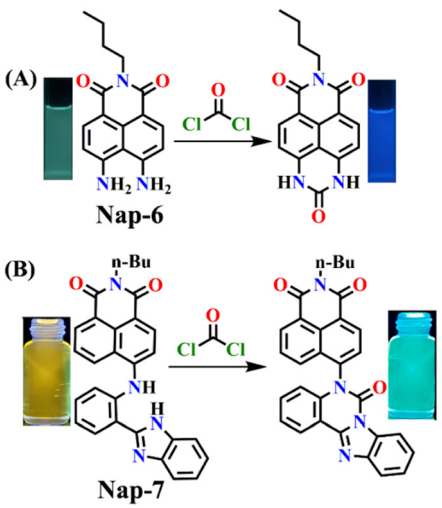

Fig. 5 (A) Structure of sensor Nap-6 and its products upon reaction with phosgene and their corresponding colorimetric images. (B) Structure of sensor Nap-7 and its products upon reaction with phosgene and their corresponding colorimetric images. Reproduced with permission from ref. 54 and 56. Copyright 2019, Willey; Copyright 2022, Elsevier.

band centered at λ = 435 nm, along with a clear isosbestic point at λ = 408 nm, was observed upon titration with phosgene. Concurrently, in the fluorescence spectra, the strong fluorescence intensity at λ = 483 nm was quenched, and the fluorescence emission shifted from green-yellow to blue, which in solution was visible to the naked eye (Fig. 5A). Furthermore, clear fluorescence color changes were observed for test strips embedded with Nap-6, in which the strip experienced a gradual shift from green-yellow to blue after being exposed to phosgene vapor for 20 minutes. This suggests that sensor Nap-6 holds promise as a potential and valuable tool for visualizing phosgene vapor in real time.

When considering ratiometric probes for the phosgene, the most common approach has been to utilize auxochromes with comparatively simple structures, such as ethylenediamine, ethanolamine, and *o*-phenylenediamine.[55] This involves forming a urea bond with the phosgene, thereby modifying the electron-withdrawing ability of the auxochromes. In 2022, a novel detection methodology was proposed by Ge *et al.* In this method, the phosgene was utilized to generate a 'fresh' Nap fluorophore.[56] This novel ratiometric probe Nap-7 was based on the use of 4-amino-1,8-naphthalimide coupled with a 2-(2-aminophenyl)benzimidazole as the reactive site. The reaction of Nap-7 with the phosgene yielded a new chromophore, where both the 4-amino moiety in the Nap and the benzimidazole were reacted, which induced ratiometric fluorescence responses between λ = 542 nm and λ = 490 nm. This large 50 nm change in the absorption in solution yielded a color change from yellow to blue (Fig. 5B) that was easily visible. Importantly, for Nap-7, the detection limit was determined to be 6.7 nM, and the fluorescence sensing response time was determined to be less than 200 s. Additionally, the Nap-7 coated test paper, and thin film formed with nanofiber morphology, exhibited both sensitive and fast sensing responses towards phosgene vapors. It is worth mentioning that the smooth surface of the thin film of Nap-7 changed to a swelled and rough surface after exposure to phosgene vapors.

Recently, Zhang and co-workers developed the fluorescent probe Nap-8, which was synthesized by incorporating an *o*-phenylenediamine derivative into a 4-pipyridine-1,8-naphthalimide fluorophore at the imide side (Fig. 6A).[57] Nap-8 was used for the detection of the phosgene in both liquid and gaseous phases. Unlike previous Nap sensors, where recognition units were directly attached to the 4-amino moiety of the Naps, potentially leading to reduced reactivity with phosgene due to steric hindrance and the involvement of the amine in the ICT, this approach aimed to enhance the sensor reactivity. Furthermore, the group was anchored onto the naphthalimide unit not through a carbon atom but *via* the para-nitrogen atom, effectively removing any steric hindrance. Through a cyclization reaction between the *o*-phenylenediamine and phosgene, a carbamide compound was formed (Fig. 6A).

This led to the generation of a more rigid structure, resulting in a noticeable enhancement in the green fluorescence emission intensity (Fig. 6B) assigned to the ICT-excited state of the sensor. Notably, no other changes were observed in the

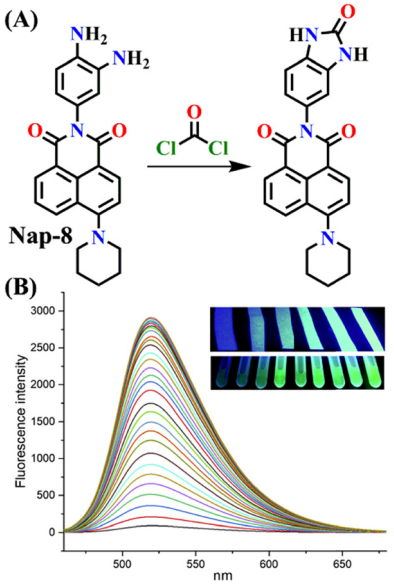

Fig. 6 (A) Structure of sensor Nap-8 and its products upon reaction with phosgene. (B) The gradual increase in the emission intensity of Nap-8 upon increasing the concentration of phosgene in the CH_2Cl_2 (inset: visual color changes in solution and gas phase after exposure to phosgene at different concentrations). Reproduced with permission from ref. 57. Copyright 2023, Elsevier.

emission band. This indicates that before the reaction, some degree of PET occurred from the electron-rich phenylenediamine to the Nap unit (which is not always observed due to the directionality in the PET mechanism for such Nap structures),[58] and as in the absence of the phosgene, Nap-8 exhibits a very weak emission at λ = 520 nm, with a primary absorption peak at λ = 410 nm. Upon the addition of the phosgene (specifically, the triphosgene containing triethylamine in CH_2Cl_2), the absorption peak was slightly red-shifted, and the fluorescence emission was enhanced drastically, as demonstrated in Fig. 6B. The initial colorless solution of Nap-8 changed to yellow after carbamide formation, and the detection limit was determined from these titrations to be 0.23 nM. Furthermore, Nap-8 exhibited exceptional selectivity for phosgene detection over other potential interfering analytes. For many of the other examples discussed above, a test paper strip incorporating Nap-8 was successfully developed for the specific detection of gaseous phosgene at low concentrations (Fig. 6B inset). These results strongly support the notion that this fluorescent probe presents a highly sensitive and cost-effective method for detecting phosgene in both liquid and gaseous phases.

Zeng and Cao developed a novel self-assembled fluorescent gel sensor, Nap-9, based on the 3,4-diamine-naphthalimide derivative.[37] Nap-9 was designed and used for the simultaneous detection of the phosgene ($COCl_2$) and thionyl chloride ($SOCl_2$) (Fig. 7A). Similar to Nap-6, a distinctive feature of Nap-9 was the presence of two inherent free NH_2 groups within the naphthalimide structure. However, unlike Nap-6, these amine units were *ortho* to each other and exhibited rapid and effective

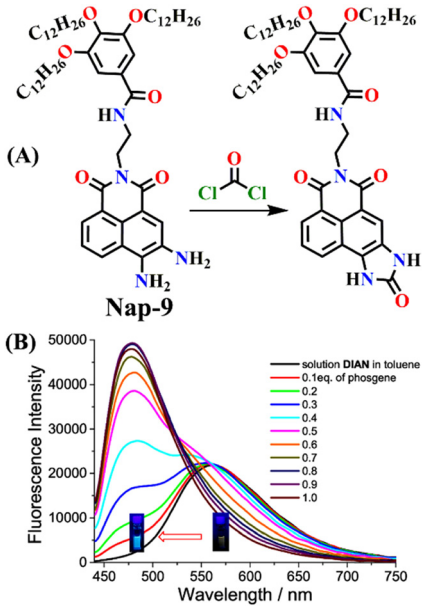

Fig. 7 (A) Structure of sensor Nap-9 and its products upon reaction with phosgene and thionyl chloride. (B) The observed changes in fluorescence emission intensity for Nap-9 after a gradual increase in phosgene concentration (inset: colorimetric photographs). Reproduced with permission from ref. 37. Copyright 2023, American Chemical Society.

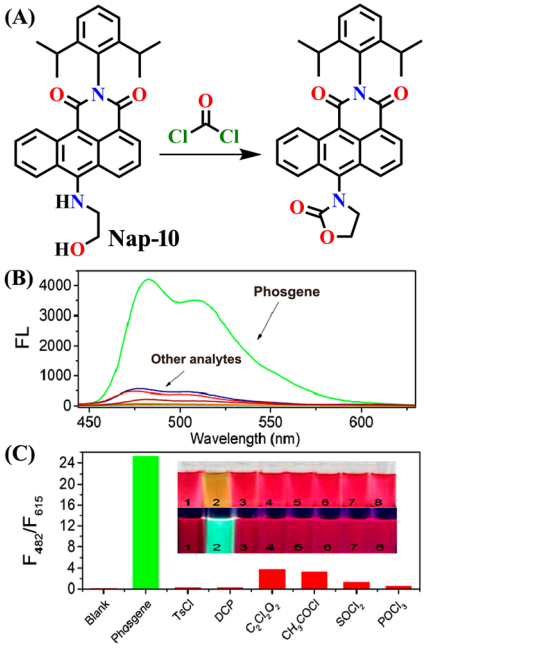

Fig. 8 (A) Structure of sensor Nap-10 and its carbamate product upon reaction with phosgene. (B) Relative changes in fluorescence emission spectra in the presence of different analytes. (C) Fluorescence intensity ratio plot for Nap-10 in response to phosgene and other analytes. Reproduced with permission from ref. 29. Copyright 2018, American Chemical Society.

acylation reactions upon exposure to the analytes. In solution, Nap-9 demonstrated high sensitivity towards the phosgene, with a low detection limit of 4.21 nM, where the UV-vis absorption spectra of Nap-9 underwent a slight hypochromatic shift from λ = 442 to 415 nm upon the addition of 2.0 equiv. of the phosgene. In contrast, the fluorescence titration demonstrated that Nap-9 also exhibited a larger hypochromatic shift from λ = 563 to 478 nm, accompanied by an enhancement in the emission intensity upon reaction with the phosgene (Fig. 7B), with striking visible color changes. This indicates that Nap-9 can detect the phosgene in a ratiometric fashion. Additionally, in toluene, the yellow-brown solution changed to ultramarine upon phosgene addition (Fig. 7B inset). Furthermore, Nap-9-based xerogel films were created for the detection of the phosgene, achieving a low detection limit of 105 ppb. Notably, the sensor demonstrated the ability to differentiate phosgene from thionyl chloride and oxalyl chloride based on their distinct response patterns. These findings provide valuable insights for the development of functional self-assembled gel sensors applicable to the detection of phosgene and other acyl chlorides.

2.2 Fluorescence sensors based on aromatic amine and hydroxyl groups as recognition units

Given that phosgene can react with both hydroxyl (OH) and amino (NH_2) groups,[59] Zeng *et al.* created the chemosensor Nap-10, which had ethanolamine as a reaction site for colorimetric and ratiometric fluorescence sensing of phosgene (Fig. 8).[29] The –NH– and –OH groups endow Nap-10 with a strong ICT character, and like Nap-9, they simultaneously react with phosgene on the occasion to form an electron-withdrawing five-membered carbamate ring with a limited ICT donor ability (Fig. 8A). The reaction of Nap-10 with the phosgene resulted in a naked-eye color change from deep red to orange, and significant changes were observed both in the absorption and fluorescence emission spectra. The initial absorption peak of Nap-10 centred at λ = 502 nm was blue-shifted to λ = 434 nm upon a gradual increase in triphosgene concentrations. In the fluorescence emission spectrum, a decrease in the emission intensity at λ = 615 nm was observed with the concurrent appearance of a new emission band at λ = 482 nm. The ratiometric fluorescence response was also clearly reflected by a sharp visual color change from red to bright green (Fig. 8B and C). Furthermore, Nap-10 exhibited excellent selectivity for the phosgene with a good response time of less than 5 minutes and a low detection limit of 2.3 nm. An easily transportable phosgene detection membrane kit was fabricated by immobilizing Nap-10 (0.125%, w/w) into polystyrene. Here, the changes observed in the solution were also observed in the polymeric state, where the deep-red color of the membrane quickly changed to a pale-yellow shade after exposure to varying concentrations of phosgene (0 to 100 ppm). These results demonstrate that Nap-10 can be a useful (naked eye) colorimetric and ratiometric fluorescence probe for the practical detection of the phosgene.

In 2019, Zeng *et al.* employed *o*-hydroxylaniline (OHA) as a recognition unit to construct the fluorescent probe Nap-11 for phosgene detection (Fig. 9).[60] The OHD moiety in Nap-11

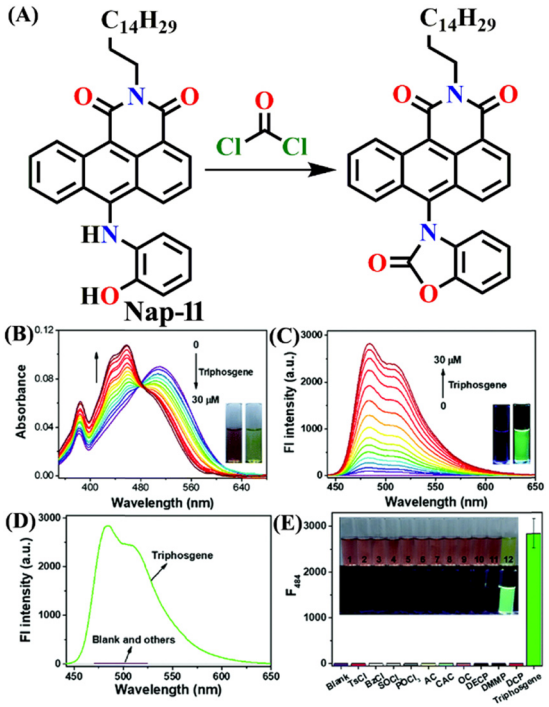

Fig. 9 (A) Structure of sensor Nap-11 and its benzoxazolinone product after reaction with phosgene. (B) Changes in UV-visible absorption and (C) fluorescence emission spectra of Nap-11 upon the addition of triphosgene in $CHCl_3$ (inset: photographs for color changes observed). (D) Relative changes in fluorescence emission for Nap-11 and (E) its corresponding selectivity plot in the presence of various analytes (inset: photographs of Nap-11 before and after the mixing of different analytes). Reproduced with permission from ref. 60. Copyright 2019, the Royal Society of Chemistry.

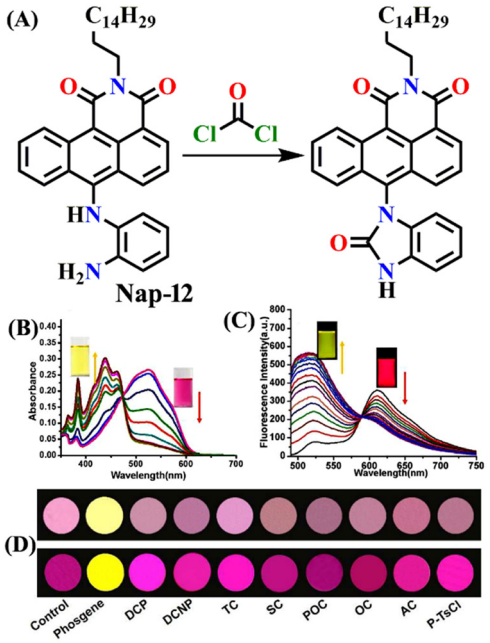

Fig. 10 (A) Structure of sensor Nap-12 and its carboximide product upon reaction with phosgene. The observed changes in (B) UV-visible absorption and (C) fluorescence emission spectra of Nap-12 after the gradual addition of the phosgene (inset: photographs of visual color changes). (D) TLC plates for color and fluorescence color changes for Nap-12 in the presence of different analytes. Reproduced with permission from ref. 61. Copyright 2019, Elsevier.

efficiently similarly reacts with phosgene as Nap-10. The corresponding product is benzoxazolinone (Fig. 9A). The reactive site here is more rigid than that in ethanolamine (aromatic *vs.* aliphatic), which facilitates the construction of a five-membered ring under low strain. Consequently, Nap-11 exhibited a fast response time of <15 s and an excellent sensitivity of 4.6 nM when exposed to the phosgene. Nap-11 displayed two characteristic absorption bands at λ = 510 nm and λ = 382 nm. When triphosgene was introduced to the Nap-11 solution (with the phosgene generated *in situ* through TEA-promoted decomposition of the triphosgene), the absorption band at λ = 510 nm gradually diminished; simultaneously, a new band emerged at λ = 458 nm, which resulted in a well-defined isosbestic point at λ = 480 nm (Fig. 9B). This transition was accompanied by a shift in color from wine red to lime, and for many of the above examples, these were visible to the naked eye. Additionally, the absorption band at λ = 384 nm experienced moderate strengthening. Phosgene induced a selective fluorescence 'turn-on' response in Nap-11 (by a factor of 920) at λ = 484 nm (Fig. 9C). This was attributed to the inhibition of the PET process from the electron-rich aniline and the weakening of the ICT effect of the OHA moiety, resulting in a distinct change in the color of the solution from purple to yellow. The mixing of other analytes into the Nap-11 solution did not cause notable changes in the fluorescence emission spectra and thus confirmed the high selectivity towards the phosgene (Fig. 9D and E). Furthermore, Nap-11 was incorporated into paper strips that displayed noticeable color and fluorescence emission changes in the presence of the phosgene, therefore enabling phosgene sensing conveniently.

2.3 Fluorescence sensors based on both aliphatic and aromatic amines as recognition units

In 2019, Liu and co-workers reported the ratiometric fluorescence probe 'Nap-12' based on the related anthracene carboximide analogue of Nap for the selective and fast detection of the phosgene with improved sensitivity (Fig. 10).[61] Nap-12 was functionalized with 1,2-diaminobenzene as a recognition moiety and could undergo an intramolecular cyclization reaction with phosgene, leading to a substantial alteration of the photophysical characteristics of Nap-12, enabling the achievement of the ratiometric fluorescent detection of phosgene (Fig. 10A). The transformation of electron-donating amino groups into electron-withdrawing carboximide groups attenuated the ICT effect similar to that observed for the Nap analogue Nap-9 above. Consequently, Nap-12 exhibited a pronounced hypsochromic shift in both the absorption and fluorescence emission spectra, transitioning from red to yellow for the latter. Notably, Nap-12 demonstrated a significant decrease in the absorption within the 490–620 nm range and an

increase in short-wavelength in the range of 380–490 nm (Fig. 10B). Nap-12 displayed a weak fluorescence emission peak at λ = 610 nm in the absence of the phosgene. However, upon reaction with the reagent, a sharp surge in the emission band centred at λ = 520 nm was observed upon the incremental addition of triphosgene (0 to 5 equiv.) (Fig. 10C). Additionally, Nap-12 displayed a fast sensing response time of fewer than 20 s, and it could detect phosgene concentrations as low as 0.09 nM. Furthermore, it was shown that Nap-12 adsorbed onto a silica TLC plate could serve as an incredibly sensitive tool for quickly identifying gaseous phosgene (Fig. 10D). Hence, Nap-12 displayed both excellent sensitivity and selectivity and additionally can be used in the sensing of phosgene through visible naked eye detection.

Another interesting type of chemosensor Nap-13 was developed for colorimetric and ratiometric fluorescence sensing of the phosgene (Fig. 11).[32] The recognition site of Nap-13 comprises one aliphatic amine and one pentacyclic aromatic amine. Here, the more nucleophilic aliphatic amine caused fast carbamylation, while the pentacyclic moiety limited the rotation of the C–N bond to increase the probability of a second carbamylation reaction taking place (Fig. 11A). When examining the spectral characteristics of Nap-13 in solution, upon introducing the triphosgene, the absorption spectra exhibit a reduction in a band centred at λ = 444 nm with the appearance of a new band at λ = 388 nm. This was accompanied by a distinct isosbestic point at λ = 409 nm (Fig. 11B). These changes were further evident in the drastic color changes observed from yellow to colorless. The fluorescence emission spectrum of Nap-13 displayed a fluorescence band from λ = 548 to 488 nm, and

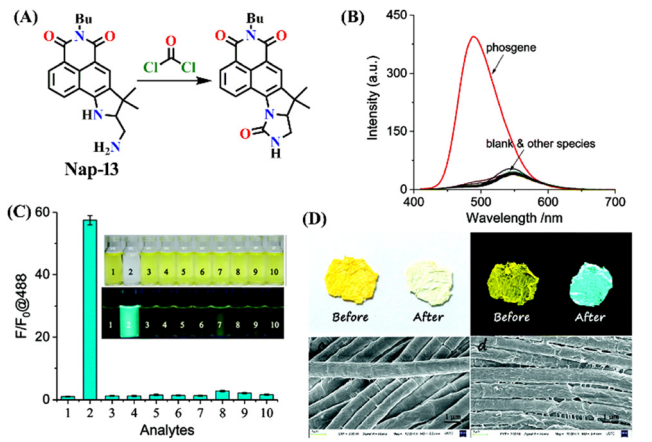

Fig. 11 (A) Structure of sensor Nap-13 and its carbamylation product obtained after reaction with phosgene. (B) Relative changes in fluorescence emission spectra of Nap-13 in the presence of different analytes and (C) corresponding selectivity plot (photos corresponding to various analytes viewed under room light and UV light) {(1) blank, (2) triphosgene (10 μM), (3) CH_3COCl, (4) $(COCl)_2$, (5) $SOCl_2$, (6) SO_2Cl_2, (7) $POCl_3$, (8) TosCl, (9) DCP, and (10) DCNP}. (D) Photographs of the fibrous membrane of Nap-13 before and after exposure to phosgene vapors and SEM images of Nap-13 before and after phosgene exposure. Reproduced with permission from ref. 32. Copyright 2019, the Royal Society of Chemistry.

the intensity for the λ_{max} at 488 nm was enhanced drastically (Fig. 11C). Concurrently, the fluorescence color of the solutions transformed from yellow to cyan. Compared to other similar sensors, Nap-13 demonstrated a quicker sensing response time of 60 s and enhanced sensitivity with a LoD of 0.3 nM. To meet the portable sensing needs, electro-spinning nanofibers loaded with Nap-13 were fabricated. The nanofiber exhibited excellent selectivity for the phosgene, offering an ultra-fast response time of less than 1 s and high sensitivity (LoD = 25 ppb) (Fig. 11D). Before phosgene exposure, the polymer fiber's surface was smooth, with uniform diameters close to 1 mm. However, after exposure to the phosgene, the surface became rough, but the diameters remained around 1 mm, as evidenced using SEM imaging (Fig. 11D). The test strip with Nap-13-embedded nanofibers turned out to be an effective tool for on-site phosgene gas detection. These results confirm that Nap-13 can effectively meet the requirements for practical applications.

Similar to Nap-10 and Nap-13, a novel fluorescent probe, Nap-14, was developed and shown to be useful for the detection of phosgene in solution and the vapor phase.[62] This probe utilizes a 4-substituted 1,8-naphthalimide unit as the fluorophore and incorporates ethylenediamine as the recognition component (Fig. 12). When exposed to the phosgene, Nap-14 underwent an intramolecular cyclization reaction leading to a significant change in fluorescence color from green to blue (Fig. 12A). For many of the examples above, this is due to a weakened ICT effect, resulting in a notable ratiometric fluorescence response (Fig. 12C). The emission intensity at λ = 505 nm being decreased concurrently with an increase in the intensity at λ = 450 nm. The absorption spectra also exhibited a clear blue shift from the absorption maxima at λ = 430 nm to 360 nm, with a clear isosbestic point at λ = 385 nm (Fig. 12B). Consequently, a color change from yellow-green to pale yellow was observed. Nap-14 showed an impressive sensitivity of LoD = 4.9 nM, as well as exceptional selectivity for phosgene over other relevant analytes. Moreover, a test paper strip containing Nap-14 was fabricated for the visual detection of low concentrations of gaseous phosgene.

Zeng and colleagues recently introduced an innovative fluorescence chemosensing platform adaptable to visualization through the use of 5G smartphones.[51] This advanced technique allows for the rapid and sensitive detection of the phosgene, with a low detection limit of 23 nM. The authors designed and synthesized Nap-15 capable of selectively sensing formaldehyde and phosgene through distinct emission channels, resulting in the formation of yellow and blue fluorescence products, respectively. The sensor utilizes hydrazine as the recognition site, which forms a three-membered cyclic amide upon reacting with the phosgene when coupled with the hydrazine (Fig. 13A). This inhibits the PET and ICT effects of the hydrazine group, leading to changes in absorption and fluorescence spectra. Upon exposure to phosgene at a concentration of 150 μM, the absorption band of Nap-15 was blue-shifted from λ = 410 nm to 394 nm. Simultaneously, the fluorescence band at λ = 503 nm gradually shifts to λ = 487 nm. Nap-15 was further

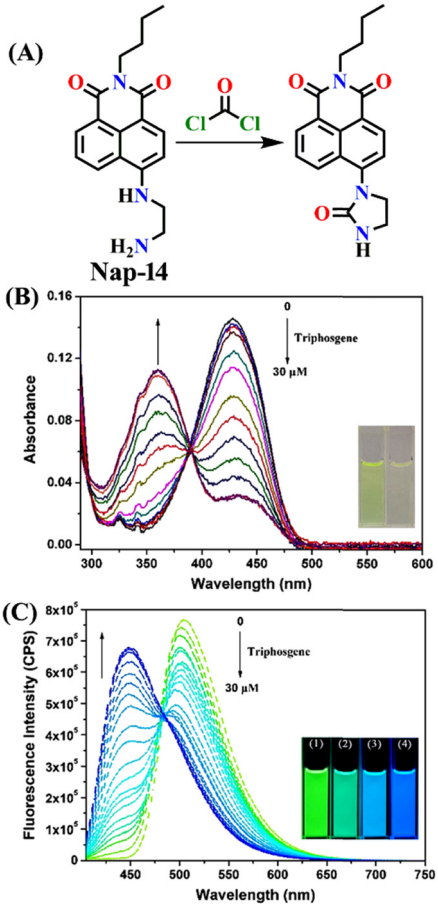

Fig. 12 (A) Structure of sensor Nap-14 and its product formed after reaction with phosgene. Relative changes in (B) UV-visible and (C) fluorescence emission spectra of Nap-14 upon increasing the triphosgene concentrations (inset: corresponding colorimetric photographs). Reproduced with permission from ref. 62. Copyright 2022, Elsevier.

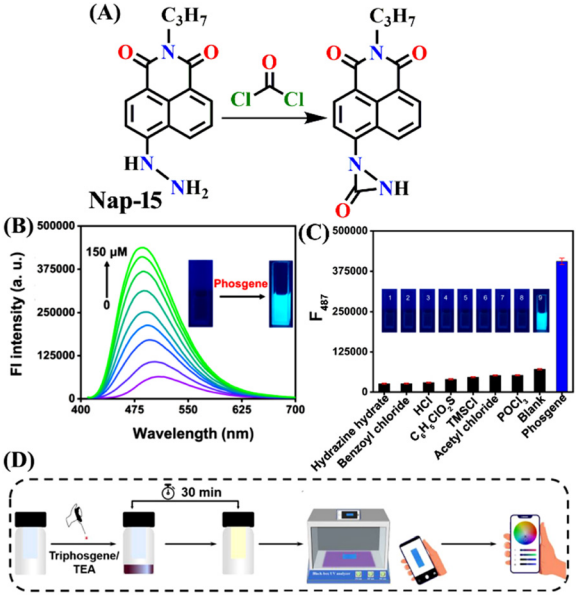

Fig. 13 (A) Structure of sensor Nap-15 and its cyclic amide product generated upon reaction with phosgene. (B) Relative changes in fluorescence emission spectra of Nap-15 upon increased addition of phosgene and (C) selectivity plot indicate phosgene's preferential binding over other analytes (inset: corresponding colorimetric photographs viewed under UV light). (D) Schematic illustration of test strip-based sensing of the phosgene using the 5G smartphone sensing platform. Reproduced with permission from ref. 51. Copyright 2023, Elsevier.

transformed into an inexpensive and portable test strip, which exhibited a fluorescence color change from dark blue to bright blue upon exposure to increasing concentrations of phosgene vapor (Fig. 13B). By utilizing a smartphone equipped with an RGB color detector, fluorescence images of the test strips could be captured and used to determine phosgene levels quantitatively (Fig. 13D). Additionally, Nap-15 demonstrated the capability to differentiate between phosgene, diphosgene, and triphosgene. Hence, in the presence of the phosgene, Nap-15 exhibited a significant fluorescence enhancement at λ = 487 nm, while the use of diphosgene and triphosgene resulted in a notable green fluorescence enhancement at λ = 508 nm (Fig. 13C). Therefore, Nap-15 can be a useful fluorescence probe for the discriminative detection of closely related acyl-chloride analytes.

Song *et al.* recently reported a series of electron donor–acceptor (D–A) types of fluorescent probes, Nap-16, Nap-17, and Nap-18, for sensitive, selective, and fast detection of the phosgene in the solution and gas phases (Fig. 14).[63] These probes have a benzoyl hydrazide as the reactive site connected to the 1,8-naphthalimide fluorophores. Different substituents were introduced at the benzoyl hydrazide to tune the photophysical and sensing performances of these sensors. Nap-16 had a CN at the *para*-position of the phenyl group, Nap-17 was unsubstituted, and Nap-18 possessed a methyl group. These probes swiftly detect the phosgene through distinctive fluorescence alterations attributed to the variation in their ICT effect, resulting in the formation of oxadiazolone derivatives *via* a specific cyclization reaction (Fig. 14A). The study examined the effect of *para*-substituents on the sensing capability and found that Nap-16 had the lowest LoD = 1.4 nM and the maximum reactivity over the other two sensors. Nap-16 also showed the fastest reaction time (5 s) and a significant change in the fluorescence from green to bright blue in the solution (Fig. 14C). The absorption spectra of Nap-16 demonstrated a decrease in absorbance at the ICT band at λ = 382 nm and the emergence of absorption at λ = 350 nm upon the addition of the triphosgene (Fig. 14B). Simultaneously, the fluorescence maximum shifted from λ = 511 nm to 424 nm, where the emission intensity at λ = 424 nm exhibited significant enhancement as a function of increasing triphosgene concentrations. Similar spectral responses were observed for Nap-17 and Nap-18, with response times of 30 s and 65 s, and LoDs of 1.7 and 8.2 nM, respectively. Additionally, test strips were fabricated using polyethylene oxide incorporating Nap-16. These enable the detection of the phosgene in the gas phase with both high selectivity and sensitivity (Fig. 14D).

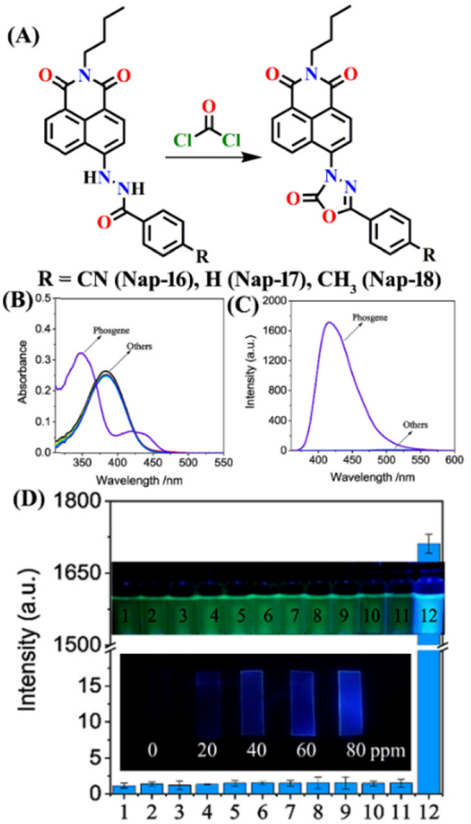

Fig. 14 (A) Structure of sensors, Nap-16, Nap-17, Nap-18, and their corresponding oxadiazolone product formed upon reaction with phosgene. Relative changes in (B) absorption and (C) fluorescence emission spectra of Nap-16 in the presence of different analytes. (D) Selectivity plot showing the preferential reaction of Nap-16 with phosgene (corresponding colorimetric images viewed under UV light and test strips showing the fluorescence color changes to different concentrations of phosgene vapors). 1, blank; 2, DCNP; 3, $(COCl)_2$; 4, $SOCl_2$; 5, SO_2Cl_2; 6, CH_3COCl; 7, $POCl_3$; 8, triphosgene; 9, diphosgene; 10, TosCl; 11, DCP; 12. Reproduced with permission from ref. 63. Copyright 2023, Elsevier.

Conclusions and outlook

In this article, we summarized and provided an overview of the current advances in the use of activity-based amino-1,8-naphthalimide fluorescence chemosensors for phosgene detection. Table 1 summarizes the fluorescence sensing properties of the different chemosensors highlighted in this article. In each section, we described the structure, sensing mechanisms, selectivity, sensitivity, and practical applications of different Nap-based fluorescence chemosensors for the phosgene. The use of Nap-based fluorescence sensors for phosgene detection is practically limitless. Nevertheless, there are several practical issues with the reported sensors illustrated in this article, and these issues have to be addressed to create practically useful fluorescence sensors for phosgene detection. Several fluorescence chemosensors reported to date operate in a single fluorescent mode, which is usually susceptible to interference and has limited analytical discrimination. However, ratiometric fluorescent sensors, which use two different fluorescence spectral windows, are more accurate and suitable for use in real-world samples by eliminating external interference through self-calibration based on the two distinct emission bands. Additionally, they demonstrate the ability to identify specific targets with precision in detailed analyses.

The phosgene sensors discussed here typically contain functional groups, such as ethylenediamine, ethanolamine, oxime, *o*-hydroxy aniline, and *o*-phenylenediamine, as recognition moiety. Fluorescent probes based on OPD react with nitric oxides (NO) to generate benzotriazoles, resulting in a fluorescence response similar to that induced by phosgene-generated urea.[63] However, these OPD-based sensors cannot differentiate between NO and phosgene, as well as their substitutes. Furthermore, the presence of an oxime group may lead to unintended interference because it can be oxidized by hypochlorous acid.[64] Systems utilizing amino or hydroxyl groups as sensing groups are susceptible to activation by substances, such as thionyl chloride and formaldehyde. Additionally, $SOCl_2$, acyl chlorides, PCl_3, $POCl_3$, and organophosphate nerve agents pose potential sources of interference in the detection of phosgene.[65] Previous studies have shown that most fluorescent probes have trouble differentiating between triphosgene and diphosgene. In this context, there is a need for an optimal sensor capable of distinguishing between these species while exhibiting the ability to detect phosgene in the presence of various interfering analytes selectively. Achieving this goal hinges on prioritizing the positioning, selection, and reactivity of the recognition groups.

Another issue to consider is the extended response times because they are mostly based on activity sensing, with certain probes taking several minutes to complete the detection process. This delay can be attributed to the prevalent use of aromatic diamine moieties, such as *o*-phenylenediamine, in the majority of reported fluorescent chemosensors. These moieties are inherently less reactive, leading to slower reactions. Conversely, chemosensors utilizing one aliphatic amine as the active site exhibit a rapid sensing reaction due to their higher nucleophilic nature. This aliphatic amine effectively catalyzes the initial reaction process. Therefore, enhancing reactivity by incorporating superior nucleophiles at the reaction site can significantly reduce reaction times. Even though the reported detection limits of some of the sensors featured herein are down to micromolar or even nanomolar levels, the sensitivity of some probes is higher than the safety threshold of the phosgene.

At present, the predominant optical probes designed for phosgene detection are typically small molecules. Although these probes exhibit a wide range of structural variations and generally perform well in detecting the phosgene in solution, they cannot detect the phosgene in the gaseous phase. Conversely, electrospinning proves to be a highly effective means for producing nano- and microfibrous membrane-based sensors.[53] These membranes offer a substantial surface area-to-volume ratio and controlled morphology. This unique nano- and microscale architecture is characterized by high

Table 1 Summary of the fluorescence sensing properties of Nap-based chemosensors discussed in this article for phosgene sensing

Structure of sensor	Structure of product	λ_{max} sensor (nm)/λ_{max} product (nm)	Sensing medium	Quantum yield (Φ)	Response time	LoD	Sensing mechanism	Ref.
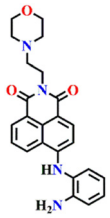 Nap-1	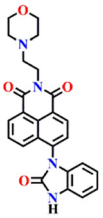	480/—	$CHCl_3$	—	<3 minute	2.8 ppb	PET	11
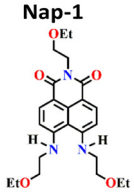 Nap-2	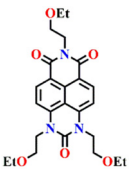	511/442	DCE	0.37	~20 minutes	1.3 nM	ICT	31
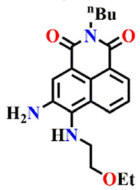 Nap-3	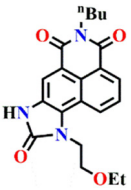	559/468	DCE	0.016	<6 minutes	0.7 nM	ICT	30
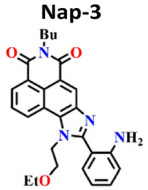 Nap-4	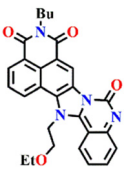	422/526	1,4-Dioxane	—	<20 s	3.2 nM	ICT	53
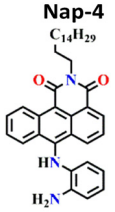 Nap-5	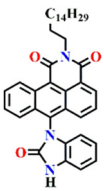	500/—	$CHCl_3$	0.65 in ethanol	<2 minutes	72 nM	ICT	8
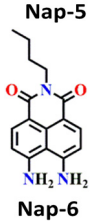 Nap-6	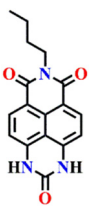	483/455, 430	CH_2Cl_2	—	20 minutes	2.25 μM	ICT	54
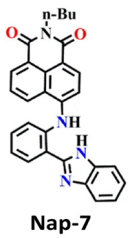 Nap-7	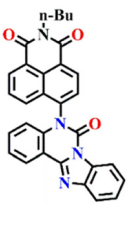	542/490	$CHCl_3$	—	—	6.7 nM	PET and ICT	56

Table 1 *(continued)*

Structure of sensor	Structure of product	λ_{max} sensor (nm)/λ_{max} product (nm)	Sensing medium	Quantum yield (Φ)	Response time	LoD	Sensing mechanism	Ref.
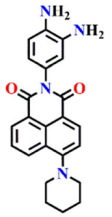 Nap-8	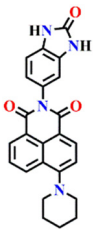	520/—	CH_2Cl_2	0.53	3 s	0.23 nM	PET and ICT	57
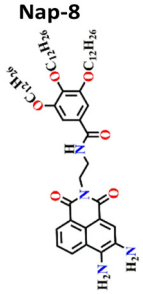 Nap-9	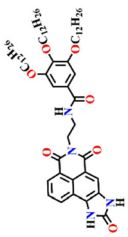	563/478	Toluene	5.18%	—	4.21 nM	ICT	37
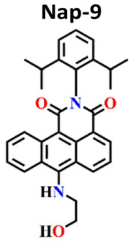 Nap-10	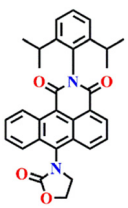	615/482	$CHCl_3$	3.3%	<5 min	2.3 nM	ICT	29
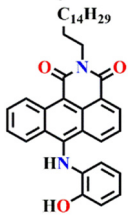 Nap-11	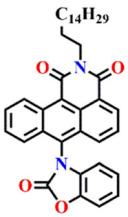	484/—	$CHCl_3$	0.06%	<15 s	4.6 nM	ICT and PET	60
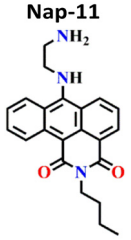 Nap-12	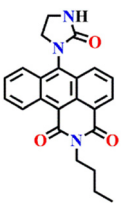	610/520	$CHCl_3$	—	—	0.09 nM	ICT	61
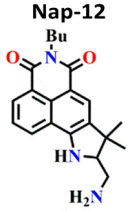 Nap-13	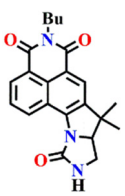	548/488	CH_3CN	0.16	60 s	0.3 nM	ICT	32

Table 1 *(continued)*

Structure of sensor	Structure of product	λ_{max} sensor (nm)/λ_{max} product (nm)	Sensing medium	Quantum yield (Φ)	Response time	LoD	Sensing mechanism	Ref.
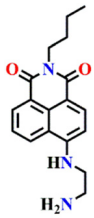 Nap-14	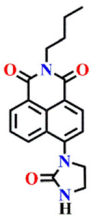	505/450	DCE	—	12 min	4.9 nM	ICT	62
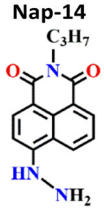 Nap-15	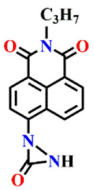	487/—	$CHCl_3$	—	—	23 nM	PET and ICT	51
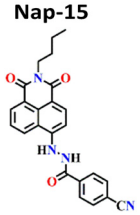 Nap-16	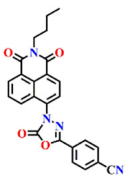	511/420	DCE	0.01	5 s	1.4 nM	ICT	63
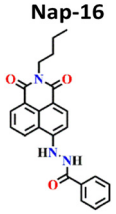 Nap-17	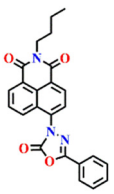	518/430	DCE	0.04	30 s	1.7 nM	ICT	63
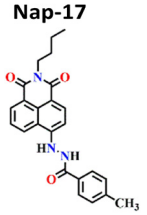 Nap-18	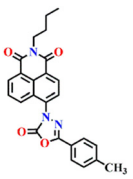	519/435	DCE	0.02	60 s	8.2 nM	ICT	63

porosity and a large surface area, which significantly enhances the potential for reducing response time and achieving high sensitivity for the detection of the phosgene. However, the size of the structures and the homogeneity of the probe with nanofibers affect the probe's detection performance, which has to be improved in the future.

Very recently, the concept of supramolecular self-assembly has become a versatile method for toxic gas sensing.[66] Utilizing supramolecular self-assembled probes holds great promise for vapor-phase phosgene monitoring. Supramolecular self-assembly probes can swiftly and effectively detect phosgene by capitalizing on nucleophilic reactions coupled with intermolecular non-covalent interactions, such as hydrogen bonding, π–π, and dipole–dipole interactions.[67] Thus, there is significant merit in advancing the development of supramolecular-assembled probes as valuable complements to the current toolkit of small molecular optical probes.[68]

In summary, we believe that this review conveys the recent advantages of the use of amino-1,8-naphthalimide-based structures in fluorescent sensing and highlights their pivotal role in phosgene detection. We anticipate that this review will prove beneficial to researchers engaged in analogous fields, inspiring new perspectives for the creation of reliable chemosensors tailored to phosgene detection in the future.

Conflicts of interest

There are no conflicts to declare.

Acknowledgements

The authors are grateful to the Indian Institute of Technology Palakkad (ERG research grant 2023-168-CHY-SHS-ERG-SP to SS), and Science and Engineering Research Board (EMEQ research grant EEQ/2023/000386 to SS), India, for financial support.

References

1 V. Kumar, H. Kim, B. Pandey, T. D. James, J. Yoon and E. V. Anslyn, *Chem. Soc. Rev.*, 2023, **52**, 663–704.
2 W.-Q. Meng, A. C. Sedgwick, N. Kwon, M. Sun, K. Xiao, X.-P. He, E. V. Anslyn, T. D. James and J. Yoon, *Chem. Soc. Rev.*, 2023, **52**, 601–662.
3 G. J. Fitzgerald, *Am. J. Public Health*, 2008, **98**, 611–625.
4 A. M. Sciuto, P. T. Strickland, T. P. Kennedy, Y. L. Guo and G. H. Gurtner, *J. Appl. Physiol.*, 1996, **80**, 149–157.
5 J. L. Plahovinsak, M. R. Perry, K. A. Knostman, R. Segal and M. C. Babin, *Inhalation Toxicol.*, 2015, **27**, 832–840.
6 W. W. Holmes, B. M. Keyser, D. C. Paradiso, R. Ray, D. K. Andres, B. J. Benton, C. C. Rothwell, H. M. Hoard-Fruchey, J. F. Dillman and A. M. Sciuto, *Toxicol. Lett.*, 2016, **244**, 8–20.
7 S. A. Cucinell and E. Arsenal, *Arch. Environ. Health*, 1974, **28**, 272–275.
8 L. T. Zeng, H. Y. Zeng, L. R. Jiang, S. Wang, J. T. Hou and J. Yoon, *Anal. Chem.*, 2019, **91**, 12070–12076.
9 H. Babad and A. G. Zeiler, *Chem. Rev.*, 1973, **73**, 75–91.
10 W. S. Wu and V. S. Gaind, *Analyst*, 1993, **118**, 1285–1287.
11 Y. Hu, L. Chen, H. Jung, Y. Y. Zeng, S. Lee, K. M. K. Swamy, X. Zhou, M. H. Kim and J. Yoon, *ACS Appl. Mater. Interfaces*, 2016, **8**, 22246–22252.
12 H. C. Xia, X. H. Xu and Q. H. Song, *ACS Sens.*, 2017, **2**, 178–182.
13 W. S. Wu and V. S. Gaind, *Analyst*, 1993, **118**, 1285–1287.
14 G. G. Esposito, D. Lillian, G. E. Podolak and R. M. Tuggle, *Anal. Chem.*, 1977, **49**, 1774–1778.
15 A. Keil, H. Hernandez-Soto, R. J. Noll, M. Fico, L. Gao, Z. Ouyang and R. G. Cooks, *Anal. Chem.*, 2008, **80**, 734–741.
16 Y. Juillet, C. Dubois, F. Bintein, J. Dissard and A. Bossée, *Anal. Bioanal. Chem.*, 2014, **406**, 5137–5145.
17 R. M. Black and R. W. Read, *J. Chromatogr. A*, 1991, **558**, 393–404.
18 M. A. K. Khan, K. Kerman, M. Petryk and H.-B. Kraatz, *Anal. Chem.*, 2008, **80**, 2574–2582.
19 F. Yan and T. Vo-Dinh, *Sens. Actuators, B*, 2007, **121**, 61–66.
20 Y. Ohrui, R. Hashimoto, T. Ohmori, Y. Seto, H. Inoue, H. Nakagaki, K. Yoshikawa and L. McDermott, *Forensic Chem.*, 2020, **21**, 100292.
21 S. Choi, Y. Jeong, Y. J. Koh, J. H. Lee, H. Nam and J. Lee, *Bull. Korean Chem. Soc.*, 2019, **40**, 279–284.
22 D. Wu, A. C. Sedgwick, T. Gunnlaugsson, E. U. Akkaya, J. Yoon and T. D. James, *Chem. Soc. Rev.*, 2017, **46**, 7105–7123.
23 R. Mondal, A. Shanmughan, A. Murugeswari and S. Shanmugaraju, *Chem. Commun.*, 2023, **59**, 11456–11468.
24 W. Feng, S. Gong, E. Zhou, X. Yin and G. Feng, *Anal. Chim. Acta*, 2018, **1029**, 97–103.
25 J. Tan, Z. Li, W. Yao, Z. Ji, Z. Sun and J. You, *Dyes Pigm.*, 2021, **187**, 109138.
26 T.-I. Kim, B. Hwang, J. Bouffard and Y. Kim, *Anal. Chem.*, 2017, **89**, 12837–12842.
27 M. Sayar, E. Karakuş, T. Güner, B. Yildiz, U. H. Yildiz and M. Emrullahoğlu, *Chem. – Eur. J.*, 2018, **24**, 3136–3140.
28 Y. Zhang, A. Peng, X. Jie, Y. Lv, X. Wang and Z. Tian, *ACS Appl. Mater. Interfaces*, 2017, **9**, 13920–13927.
29 Q. Hu, C. Duan, J. Wu, D. Su, L. Zeng and R. Sheng, *Anal. Chem.*, 2018, **90**, 8686–8691.
30 S. L. Wang, L. Zhong and Q. H. Song, *Chem. – Eur. J.*, 2018, **24**, 5652–5658.
31 S. L. Wang, L. Zhong and Q. H. Song, *Chem. Commun.*, 2017, **53**, 1530–1533.
32 S. L. Wang, C. L. Zhang and Q. H. Song, *J. Mater. Chem. C*, 2019, **7**, 1510–1517.
33 Y. Li, J. Zhang, Z. Liang, R. Yang, L. Qu, Z. Li and Y. Sun, *Sens. Actuators, B*, 2023, **376**, 132971.
34 M. Du, B. Huo, J. Liu, M. Li, A. Shen, X. Bai, Y. Lai, L. Fang and Y. Yang, *J. Mater. Chem. C*, 2018, **6**, 10472–10479.
35 Q. Han, Q. Wang, A. Gao, X. P. Chang, L. Zeng and X. Cao, *ACS Sustainable Chem. Eng.*, 2023, **11**, 2139–2150.
36 Y. L. Huang, W. Ye, Y. T. Su, Z. Y. Wu and H. Zheng, *Dyes Pigm.*, 2020, **173**, 107854.
37 Q. Han, Q. Wang, A. Gao, X. P. Chang, L. Zeng and X. Cao, *ACS Sustainable Chem. Eng.*, 2023, **11**, 2139–2150.
38 S. Tal, H. Salman, Y. Abraham, M. Botoshansky and Y. Eichen, *Chem. – Eur. J.*, 2006, **12**, 4858–4864.
39 D. Wu, A. C. Sedgwick, T. Gunnlaugsson, E. U. Akkaya, J. Yoon and T. D. James, *Chem. Soc. Rev.*, 2017, **46**, 7105–7123.
40 C. Wu, H. Xu, Y. Li, R. Xie, P. Li, X. Pang, Z. Zhou, B. Gu, H. Li and Y. Zhang, *Talanta*, 2019, **200**, 78–83.
41 W. Tuo, J. Bouquet, F. Taran and T. Le Gall, *Chem. Commun.*, 2019, **55**, 8655–8658.
42 J. M. Delente, D. Umadevi, S. Shanmugaraju, O. Kotova, G. W. Watson and T. Gunnlaugsson, *Chem. Commun.*, 2020, **56**, 2562–2565.
43 B. Mohan, M. K. Noushija and S. Shanmugaraju, *Tetrahedron Lett.*, 2022, 154155.
44 H. Q. Dong, T. B. Wei, X. Q. Ma, Q. Y. Yang, Y. F. Zhang, Y. J. Sun, B. B. Shi, H. Yao, Y. M. Zhang and Q. Lin, *J. Mater. Chem. C*, 2020, **8**, 13501–13529.
45 S. Shao, D. Zhang, B. Lin and Y. Han, *Spectrochim. Acta, Part A*, 2023, **303**, 123284.
46 S.-H. Park, N. Kwon, J.-H. Lee, J. Yoon and I. Shin, *Chem. Soc. Rev.*, 2020, **49**, 143–179.
47 S. Banerjee, E. B. Veale, C. M. Phelan, S. A. Murphy, G. M. Tocci, L. J. Gillespie, D. O. Frimannsson, J. M. Kelly and T. Gunnlaugsson, *Chem. Soc. Rev.*, 2013, **42**, 1601–1618.
48 B. Mohan, D. Umadevi and S. Shanmugaraju, *Sens. Diagn.*, 2023, **2**, 262–267.
49 B. Mohan, N. M. Kunhumon and S. Shanmugaraju, *Sens. Diagn.*, 2023, **2**, 1158–1175.
50 H.-Q. Dong, T.-B. Wei, X.-Q. Ma, Q.-Y. Yang, Y.-F. Zhang, Y.-J. Sun, B.-B. Shi, H. Yao, Y.-M. Zhang and Q. Lin, *J. Mater. Chem. C*, 2020, **8**, 13501–13529.

51 H. Ye, Y. Ke, C. Yue, P. Xie, R. Sheng and L. Zeng, *Dyes Pigm.*, 2022, **207**, 110782.
52 L. Wu, A. C. Sedgwick, X. Sun, S. D. Bull, X.-P. He and T. D. James, *Acc. Chem. Res.*, 2019, **52**, 2582–2597.
53 S. L. Wang, C. Li and Q. H. Song, *Anal. Chem.*, 2019, **91**, 5690–5697.
54 W. Zhou, Q. Chen, A. Wu, Y. Zhang and W. Yu, *J. Chin. Chem. Soc.*, 2020, **67**, 1213–1218.
55 B. Liu, M. Zhou, Y. Huang, B. Du, L. Wang, Z. Xu, T. Qin and X. Peng, *Spectrochim. Acta, Part A*, 2022, **281**, 121619.
56 J. Y. Ni, D. L. Qian, R. Sun, C. X. Qin and J. F. Ge, *Talanta*, 2022, **236**, 122826.
57 Y. Zhang, X. Qiu, B. Wang, X. Liu, Y. Cheng, X. Rong, Y. Kuang, L. Sun, J. Liu, R. L. Luck and H. Liu, *Spectrochim. Acta, Part A*, 2023, **289**, 122189.
58 M. Martínez-Calvo, S. A. Bright, E. B. Veale, D. C. Williams and T. Gunnlaugsson, *Front. Chem. Sci. Eng.*, 2020, **14**, 61–75.
59 K. Maiti, D. Ghosh, R. Maiti, V. Vyas, P. Datta, D. Mandal and D. K. Maiti, *J. Mater. Chem. A*, 2019, **7**, 1756–1767.
60 L. Zeng, H. Zeng, S. Wang, S. Wang, J. T. Hou and J. Yoon, *Chem. Commun.*, 2019, **55**, 13753–13756.
61 P. Liu, N. Liu, C. Liu, Y. Jia, L. Huang, G. Zhou, C. Li and S. Wang, *Dyes Pigm.*, 2019, **163**, 489–495.
62 Z. Xu, Y. Luo, Y. Hong, Z. Liu, M. X. Zhang, S. X. Gu and J. Yin, *Spectrochim. Acta, Part A*, 2022, **269**, 120789.
63 X. L. Miao, W. Feng and Q. H. Song, *Dyes Pigm.*, 2023, **216**, 111348.
64 M. J. Plater, I. Greig, M. H. Helfrich and S. H. Ralston, *J. Chem. Soc., Perkin Trans. 1*, 2001, 2553–2559.
65 Q. Ye, S. Ren, H. Huang, G. Duan, K. Liu and J.-B. Liu, *ACS Omega*, 2020, **5**, 20698–20706.
66 A. Leggio, E. L. Belsito, G. De Luca, M. L. Di Gioia, V. Leotta, E. Romio, C. Siciliano and A. Liguori, *RSC Adv.*, 2016, **6**, 34468–34475.
67 A.-M. Andringa, M.-J. Spijkman, E. C. P. Smits, S. G. J. Mathijssen, P. A. van Hal, S. Setayesh, N. P. Willard, O. V. Borshchev, S. A. Ponomarenko, P. W. M. Blom and D. M. de Leeuw, *Org. Electron.*, 2010, **11**, 895–898.
68 A. J. Savyasachi, O. Kotova, S. Shanmugaraju, S. J. Bradberry, G. M. OMaille and T. Gunnlaugsson, *Chem*, 2017, **3**, 764–811.